Analyzing Blood Cells of High-Risk Myelodysplastic Syndrome Patients Using Interferometric Phase Microscopy and Fluorescent Flow Cytometry

Itay Barnea *, Lior Luria , Arik Girsault , Ofira Dabah , Matan Dudaie , Drorit Merkel , Natan T Shaked

Posted Date: 22 January 2024

doi: 10.20944/preprints202401.1554.v1

Keywords: myelodysplastic syndromes (MDS); interferometric phase microscopy (IPM); hematology

Article

Analyzing Blood Cells of High-Risk Myelodysplastic Syndrome Patients Using Interferometric Phase Microscopy and Fluorescent Flow Cytometry

Itay Barnea [1,*], Lior Luria [1], Arik Girsault [1], Ofira Dabah [1], Matan Dudaie [1], Drorit Merkel [2,3] and Natan T. Shaked [1]

[1] Department of Biomedical Engineering, Tel Aviv University, Tel Aviv, Israel; itay.barnea.1@gmail.com (I. B.); iiorluria@mail.tau.ac.il (L. L.); arikgirsault@tauex.tau.ac.il (A. G.); ofiradabahyo@tauex.tau.ac.il (O. D.); matan.dudaie@gmail.com (M. D.); nshaked@tauex.tau.ac.il (N. T. S.)

[2] MDS Center, Sheba Medical Center, Ramat Gan, Israel ; drorit.merkel@sheba.health.gov.il (D. M.)

[3] Faculty of Medicine, Tel Aviv University, Tel Aviv, Israel

* Correspondence: itay.barnea.1@gmail.com

Abstract: (1) Background: Myelodysplastic syndromes (MDS) are a group of diseases that affect the morphology and function of neutrophils. Rapid diagnosis of MDS is crucial for the initiation of treatment that can vastly improve disease outcome. (2) methods: In this work, we present a new approach for detecting morphological differences between neutrophils isolated from blood samples of high risk MDS patients and that for patients and blood bank donors (BBDs). First, using fluorescent flow cytometry CD66b positive cells were stained with 2′,7′-dichlorofluorescin diacetate (DCF) and Hoechst. Secondly, we imaged the cells using interferometric phase microscopy (IPM) without utilizing cell staining. (3) Results: flow cytometry results show MDS patients present different dispersion patterns compared to BBDs. BBDs present two distinct subpopulations (one of these are the H cells constituting 16% for neutrophils) whereas MDS patients present only 4% of this subpopulation. IPM results are consistent with this pattern: ~20% of BBDs neutrophils were characterized as H cells and whereas MDS patients present only ~4% of these cells. (5) Conclusion- IPM can be utilized for diagnosis of complex hematological pathologies such as MDS.

Keywords: myelodysplastic syndromes (MDS); interferometric phase microscopy (IPM); hematology

1. Introduction

Myelodysplastic syndromes (MDS), also known as myelodysplastic neoplasms are a group of hematopoietic malignancies characteristic by marrow dysplasia, with failure of bone marrow stem cells to mature into normal-functioning blood cells. Patients diagnosed with MDS present with anemia, neutropenia, and thrombocytopenia along with morphologic dysplastic bone marrow and increased risk of acute myeloid leukemia (AML) [1]. Often these patients suffer from fatigue, recurrent infections and bleeding.

The incidence of new MDS diagnosis in the United States is about 4 in 100 thousand per year [1], and the 5-year life expectancy of MDS patients is about 37% [2]. MDS affects mostly elderly patients with a median age of diagnosis of approximately 70 years, thus the incidence rate increases from 4 to 25 per 100 thousand above the age of 65. MDS are broadly divided into patients with high and low risk to undergo transformation to AML. High risk patients are typically characterized by worse anemia, neutropenia, or thrombocytopenia a higher percentage of myoblasts as well as genetic variants associated with a worse prognosis [3].

The clinical manifestation of MDS is influenced by the functional deficiencies in the particular blood cells. For example, MDS patients with maturational defects of megakaryocytes are correlated to bleeding independently of thrombocytopenia [4]. Similarly, infections are a major cause of illness

 doi:10.20944/preprints202401.1554.v1

and death in MDS patients [5], both in patients with neutrophil dysfunction and in patients with neutropenia [6]. Morphological and physiological abnormalities are major attributes of neutrophils in MDS, including nuclear hyper-segmentation, cytoplasmic hypo-granularity [7] and reduction in reactive oxygen species (ROS) that are essential for the management of pathogens [8].

The current protocol for the diagnosis of MDS includes bone marrow aspiration after anemia thrombocytopenia or neutropenia that persists for 6 months or more [9], thus, even at the most favorable circumstances patients will obtain diagnosis and start treatment many months after the onset of symptoms. Unfortunately, in some cases, rapid diagnosis and treatment are critical to prevent deterioration in the health of patients. For example, some MDS patients are at high risk of developing AML. These patients may benefit from bone marrow transplantation that may prevent this deadly disease [10].

2′,7′-dichlorodihydrofluorescein diacetate, also known as DCF, is a cell-permeable molecule that becomes fluorescent in the presence of ROS [11]. DCF has been used to characterize the presence and distribution of ROS in different living cells including neutrophils. In neutrophils, the level of DCF fluorescence is correlated to the initiation of an immune response to a microorganism stimulation [12-13].

Interferometric phase microscopy (IPM), also known as digital holographic microscopy or quantitative phase microscopy, is a stain-free imaging technique that captures both the amplitude and phase profiles of the light that passes through transparent biological cells. IPM provides a quantitative measurement of the optical path delay (OPD) at each point in the sample, where OPD is defined as the difference between the integral refractive index of the sample and that of the surrounding medium multiplied by the sample thickness. These quantitative quasi-three-dimensional phase images enable the calculation of 3D parameters such as the cellular dry mass, in addition to 2D parameters such as cell area [14-15].

IPM technologies have been used to distinct different types of cells by us and by other groups, for example to distinct between normal and abnormal sperm cells [16] between different leucocytes [17] and between normal and pathological hematopoietic cells such as acute myeloid leukemia (AML) myeloproliferative neoplasm (MPN) [18].

In this work, we present a new way to detect MDS by imaging neutrophils by IPM. This research aims to show that in healthy donors two neutrophil populations are present in the OPD images, whereas in MDS patients only one population is present, which can then be used for MDS detection.

2. Materials and Methods

2.1. Blood acquisition

High-risk MDS patient blood was acquired from the Hemato-oncology Department of Sheba Medical Center, Ramat Gan, Israel. This study was approved by the Sheba Medical Center (approval number 8374-21-SMC) and the Tel Aviv University ethical review boards (approval number 003618-3) . MDS patients signed informed consent forms before participating in the study, Blood tubes were coded by numbers in order to preserve the anonymity of the donors. Venous blood was drawn from MDS patients during regular follow-up treatment and placed in tubes containing EDTA.

As a control group, EDTA-supplemented blood samples from healthy blood bank donors (BBDs) were acquired from the Israeli blood bank, Magen David Adom, Tel Hashomer Hospital, Israel. In all cases, the blood was stored at 4 °C in tubes containing EDTA and tested within 24 hours of being drawn.

2.2. Neutrophil isolation

Neutrophils were isolated using the EasySep Direct Human Neutrophil Isolation Kit (StemCell technologies, #19666). In short, 0.5 ml of blood were placed in round-bottom polystyrene 1.5 ml tubes, where the blood was combined with 50 µl of isolation cocktail and 50 µl of magnetic beads. The mixture was then incubated at room temperature for 5 min, and combined with 3.5 ml of PBS supplemented with 1 mM EDTA. After incubation, the tube was placed in a magnet (EasySep, #18000)

 doi:10.20944/preprints202401.1554.v1

for 5 min, and the liquid was poured into a new tube. Next, 20 µl of isolation cocktail and 50 µl magnetic beads were added to the tube, and after 5 min of incubation, the tube was placed in the magnet for 5 min, and the liquid was poured into a new tube and centrifuged at 1250 RPM, the supernatant was discarded and the cells were resuspended in PBS-EDTA. Cells used for flow cytometry were resuspended in a fluorescent dye mix (see flow cytometry), cells used for imaging in IPM were resuspended in PBS-EDTA supplemented with 2% paraformaldehyde (PFA) fixative, needed to prevent morphological changes in cells such as degranulation, and 7 µg/ml Hoechst 33342 (for nucleus staining).

2.3. Flow cytometry

Characterization of cells was performed by two methods of flow cytometry: analytical flow cytometry and flow cytometry that includes cell sorting. In both cases, cells were first stained with 7 µg/ml Hoechst 33342 (Sigma-Aldrich #B2261) for DNA stain, 2.5 µg/ml 2',7'-Dichlorofluorescein diacetate (DFC) (Sigma-Aldrich, #D6883) for ROS stain, and 5 µl/ml PE-conjugated anti-human CD66b Antibody (305106, Bio legend) in PBS supplemented with 1 mM EDTA for the staining of neutrophils. The cells were incubated with the staining solution at room temperature for 30 min before analysis.

For analytical flow cytometry, we used the Cytoflex 5L (Beckman Coulter) system, while for fluorescence- activated cell sorting (FACS) the BD FACSAria III (BD Biosciences) system was used.

In flow cytometry with sorting, the sorted cells were collected into a 15 ml tube containing paraformaldehyde (PFA). The final concentration of PFA in the sorted cells was ~1%. After sorting, the cells were spun at 1000 RPM, placed in a glass chamber and imaged by IPM, brightfield microscopy and fluorescent microscopy. Analysis was performed by the Kaluza analysis software 2.2 (Beckman Coulter).

2.4. Optical system

The optical system is shown in Figure 1. It is designed to flow cells through the optical system in a controlled manner and to capture images of the cells using IPM by low-coherence shearing interferometry as described in our earlier works [19] and [20]. The system also contains fluorescent microscopy and brightfield microscopy based on the Olympus IX83 inverted microscope.

For capturing IPM images, we used low-coherence shearing interferometry with constant off-axis angle (LC-SICA) module. A supercontinuum laser (SuperK EXTREME, NKT) beam with wavelength of 630±3 nm illuminates the sample as plane wave. The sample is imaged with a microscope objective lens (MO) (Olympus PlanApo N 60×/1.42 oil) and a tube lens TL (focal length 200 mm), and the image beam then pass to the external LC-SICA module. As shown in Figure 1, the LC-SICA module consists of a diffraction grating (DG) with 100 lines/mm, generating two laterally shifted sample beams. The diffracted beams are optically Fourier transformed by lens L1 (focal length 150 mm). Mask M is placed at the conjugate Fourier plane to select only the zeroth and first diffraction orders, and a glass plate phase compensator is positioned in the path of the first order. Then the two orders are projected onto lens L2 (focal length 300 mm), with L1 and L2 arranged in a 4f imaging configuration. Finally, both beams overlap on the sensor plane of the camera (Thorlabs DCC1545M-GL, 8-bit monochromatic CMOS, 1280 × 1024 pixels of 5.2 µm), creating the off-axis interferogram, captured as an 8-bit BMP image.

The complex wavefront image was reconstructed from the off-axis interferogram, and the phase of the complex wavefront was extracted and converted to the sample OPD map, such that the value at each point in the OPD map was the product of the difference between the refractive index of the sample to that of the medium and the physical height of the sample at that point. The process for the conversion of interferogram to OPD maps is described in [21].

In the resulting OPD maps, the cell area was isolated by a simple threshold, followed by a morphological dilation. Thus, we created a dataset containing the OPD information across the cell areas only. From these maps, we calculated different 3D morphological parameters such as dry mass and the average OPD, and from the threshold maps we also calculated 2D morphological parameters

 doi:10.20944/preprints202401.1554.v1

such as the cell area and the cell perimeter. The IPM-based morphological features are based on our previous works [15, 17]. In short, the OPD at a given point ($OPD_{(x,y)}$) is defined as a multiplication of the interval between the refractive index of the object $n_{o(x,y)}$ to that of the medium n_m and thickness of the object at that point ($h_{o(x,y)}$):

$$OPD_{(x,y)} = \left(n_{o(x,y)} - n_m\right) \times h_{o(x,y)}.$$

The average OPD (⟨OPD⟩) is the sum of all OPD values of a given cell, divided by the number of pixels in the cell's projection area.

The cellular dry mass (M) is defined as:

$$M = \frac{S_C}{\alpha} \times \langle \mathrm{OPD} \rangle,$$

where α is the refractive increment and approximated as 0.19 μm³/pg, S_C is the projected cell area on the x-y plane.

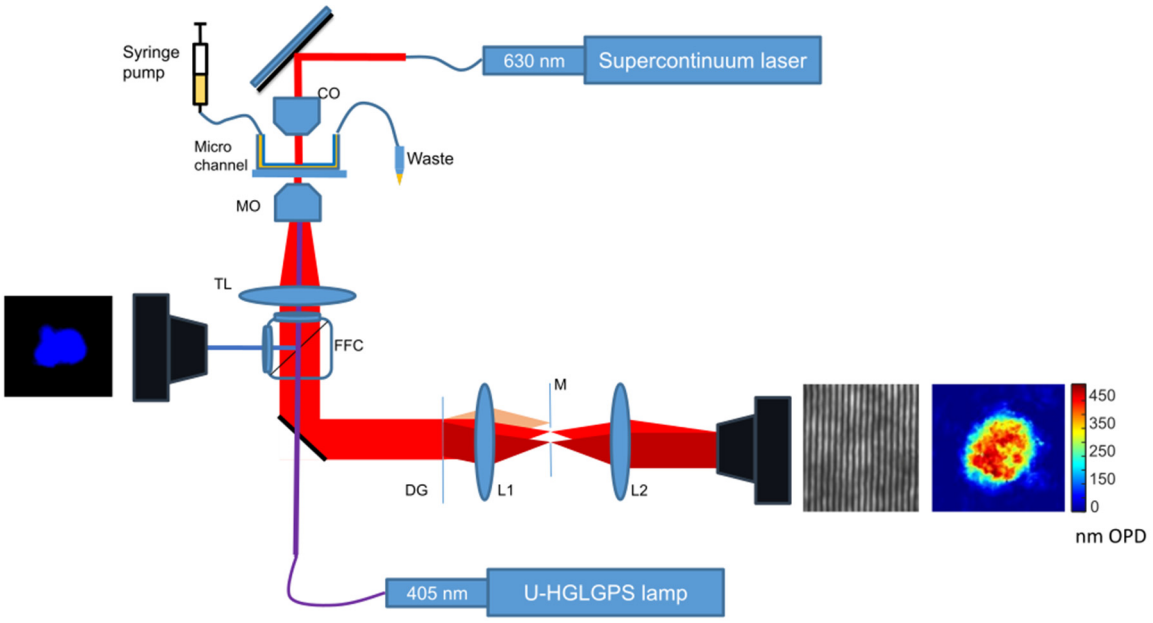

Figure 1. System configuration. The system is based on an inverted microscope, cells stained with Hoechst 33342 are pumped into a microchannel. The cell sample is illuminated by a supercontinuum laser source coupled to an acousto-optic tunable filter. The cells are magnified by a 60x oil objective and an interferogram is acquired by the LC-SICA module. In addition, cells are simultaneously imaged by fluorescent or brightfield microscopy by a different camera. CO: condenser; MO: microscope objective; TL: tube lens; FFC: Fluorescent Filter Cube; L1, L2: lenses; DG: diffraction grating; M: mask.

In addition to IPM imaging, the Olympus IX83 was also used to capture fluorescent images of the sample simultaneously to the IPM imaging. The light source used for fluorescent imaging was a 130 W Mercury Lamp Housing with Fiber (U-HGLGPS). The beam passes a Fluorescent Filter Cube (FFC), illuminates the sample through the microscope objective lens, and then the fluorescent light returns to the FFC and is projected onto the microscope camera (Basler acA2440-75um, USB 3.0). The FFC was set to match the fluorophore used; For Hoechst, FCC with an excitation filter of 325-375 nm and an emission filter of 435-485 nm was used. For FCD, an FCC with an excitation filter of 450–490 nm and an emission filter of 500–540 nm was used.

In order to image immobile cells, a glass chamber was built from a #1 60×22 mm coverslip, covered by a #1 22×22 coverslip. The two coverslips were separated by two 22-mm-long sections of a #1 coverslip. The chamber components were bonded together by melted candle wax, creating an empty chamber with a glass floor and roof with open entrances on two opposing sides and a height

 doi:10.20944/preprints202401.1554.v1

approximately equals to the thickness of a single #1 coverslip. After the addition of the liquid containing the cells, the chamber entrances on the sides were sealed by melted candle wax to prevent leakage and evaporation.

For imaging flowing cells, the cells were pumped by a two-channel programmable syringe pump (New Era Pump Systems, NE-4000) through a microchannel with a height of 0.1 mm (Ibidi μ-Slide VI 0.1). In order to identify the flowing cells, in parallel to imaging the cells with IPM, the cells were simultaneously imaged by a fluorescent microscope (using tsshe UV FFC for the Hoechst stain).

2.5. Statistical analysis

Morphologic characteristics of cells captured by IPM were extracted from the OPD maps, quantified and listed in a table. The statistical significance of the difference between two populations of cells for each characteristic was determined by two-sample t-test, which is the statistical significance for the difference of proportion between two populations was determined by two-samples independent proportions test. Results were considered statistically significant for values of $p<0.05$. Statistical images were generated using Graphpad Prism 9 (GraphPad Software, San Diego, CA).

3. Results

3.1. Analytical flow cytometry

Neutrophils from blood samples of high-risk MDS patients and healthy BBDs were stained with Hoechst, DFC and PE-CD66b. Cells were analyzed either by the BD FACSAria III or by the Cytoflex 5L systems. Cells are presented on DFC vs. Hoechst dot plot charts (Figure 2 A and B). When the PE-αCD66b conjugate was used, cells were gated to CD66b positive cells; otherwise, the cells were gated by the FSC vs. SSC dot plot to include only granulocytes. The threshold for the distinction between H and L cells (explained in "Cell Sorting") was 104 for the FACSAria III and 105 for the Cytoflex 5L system, respectively, on the Hoechst axis. The arbitrary fluorescent values of two machines can be calibrated with one another by comparing the ratio of Hoechst fluorescence in the H to L cells analyzed in the different machines.

The difference between the percentage of H cells in the two groups (18.5% in BBDs vs. 3.4% in MDS patients) is statistically significant ($p<0.01$). Moreover, dot-plot results indicate that in the MDS group there is no distinct subpopulation of cells above the thresholds (except for the MDS7b). Interestingly, the same patient, MDS-7, was tested twice, where in the second time (MDS7b) blood was drawn shortly after the patient underwent a blood transfusion. In this second sample, a high percentage of H cells was detected, leading us to speculate that these cells were exogenous to the patient.

 doi:10.20944/preprints202401.1554.v1

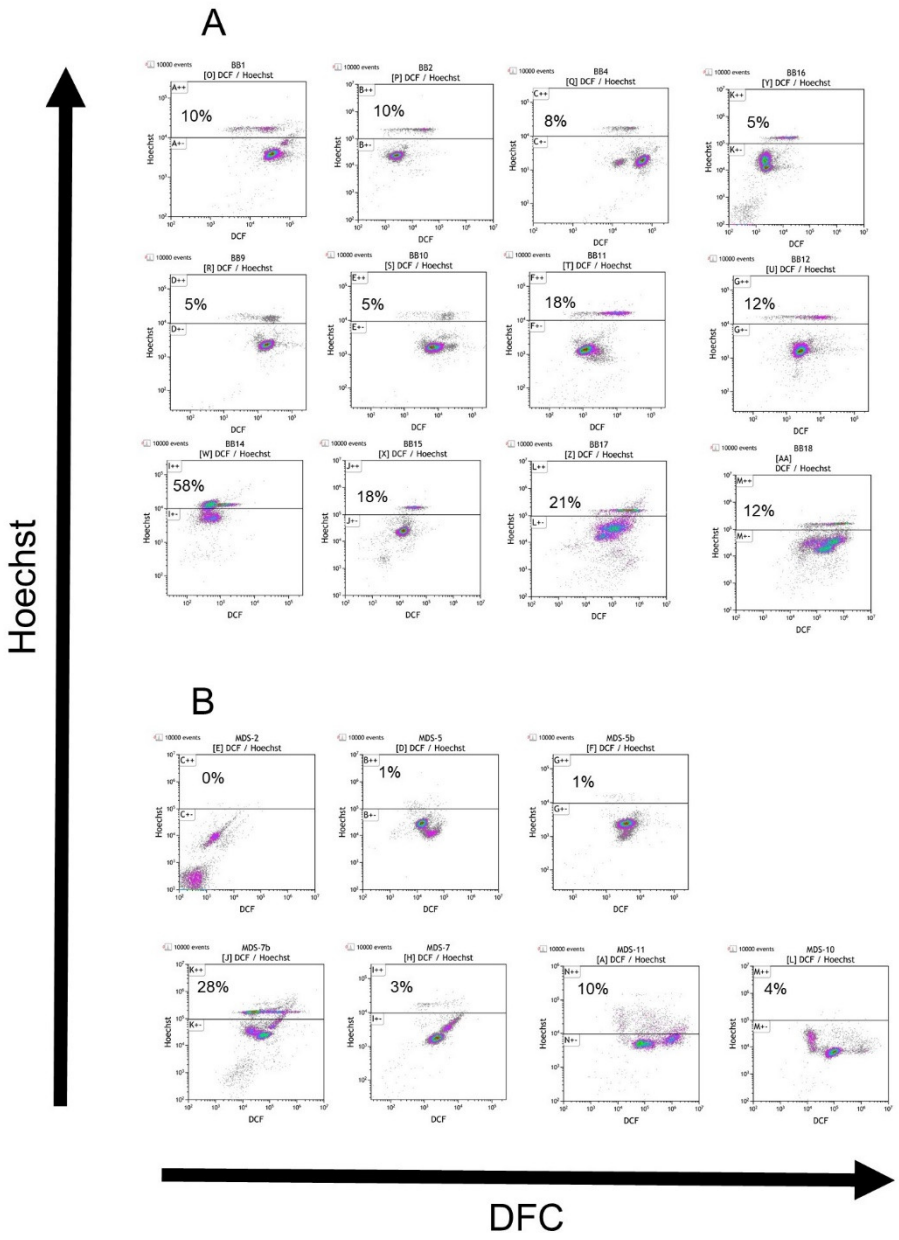

Figure 2. DFC/Hoechst dot plot of neutrophils isolated from healthy BBDs (A) or from MDS patients (B). Cells are presented after gating to CD66b positive cells (using PE-αCD66b antibody) or to granulocytes using FSC vs. SSC dispersion dot plot. Results indicate that healthy BBDs present two distinct subpopulations of cells, separated by the Hoechst level. The percentage of H cells (cells above the threshold line) are presented in each plot. The average percentage of H cells in the BBD group is 16% compared with 4% in the MDS patients group. The difference between the two groups is statistically significant ($p<0.05$).

3.2. Cell sorting

Neutrophils from four healthy donors were negatively isolated. The cells were stained by PE-CD66b, Hoechst and DCF. Using BD FACSAria III, the cells were gated to CD66 positive cells and were displayed on a DCF vs. Hoechst dot plot. Two clusters of cells appear on the plot (Figure 3A and B): a cluster with high Hoechst expression and a cluster with low Hoechst expression. These clusters were designated as H and L cells. The cells were isolated from the two clusters and pumped into two different tubes containing PFA as a fixative. After the cells were concentrated by a gentle spin (1000 RPM) and sealed in a glass chamber, the chamber was placed in the optical system and

 doi:10.20944/preprints202401.1554.v1

imaged by IPM. In addition, some of the cells were imaged by fluorescence and brightfield microscopy.

Fluorescent image analysis of the captured cells shows that H cells are represented by a round or banded nucleus (visualized by Hoechst binding to DNA) and granules of ROS (visualized by DFC fluorescent dye). In contrast, L cells are characterized by a mature, polymorphonuclear nucleus and a low level of ROS in the cytoplasm. Moreover, IPM results show that H cells display higher OPD in the cytoplasm than in the nucleus, whereas L cells in have higher OPD in the nucleus than in the cytoplasm. Interestingly, granules that include ROS and are stained by DFC display localized high OPD levels (Figure 3B).

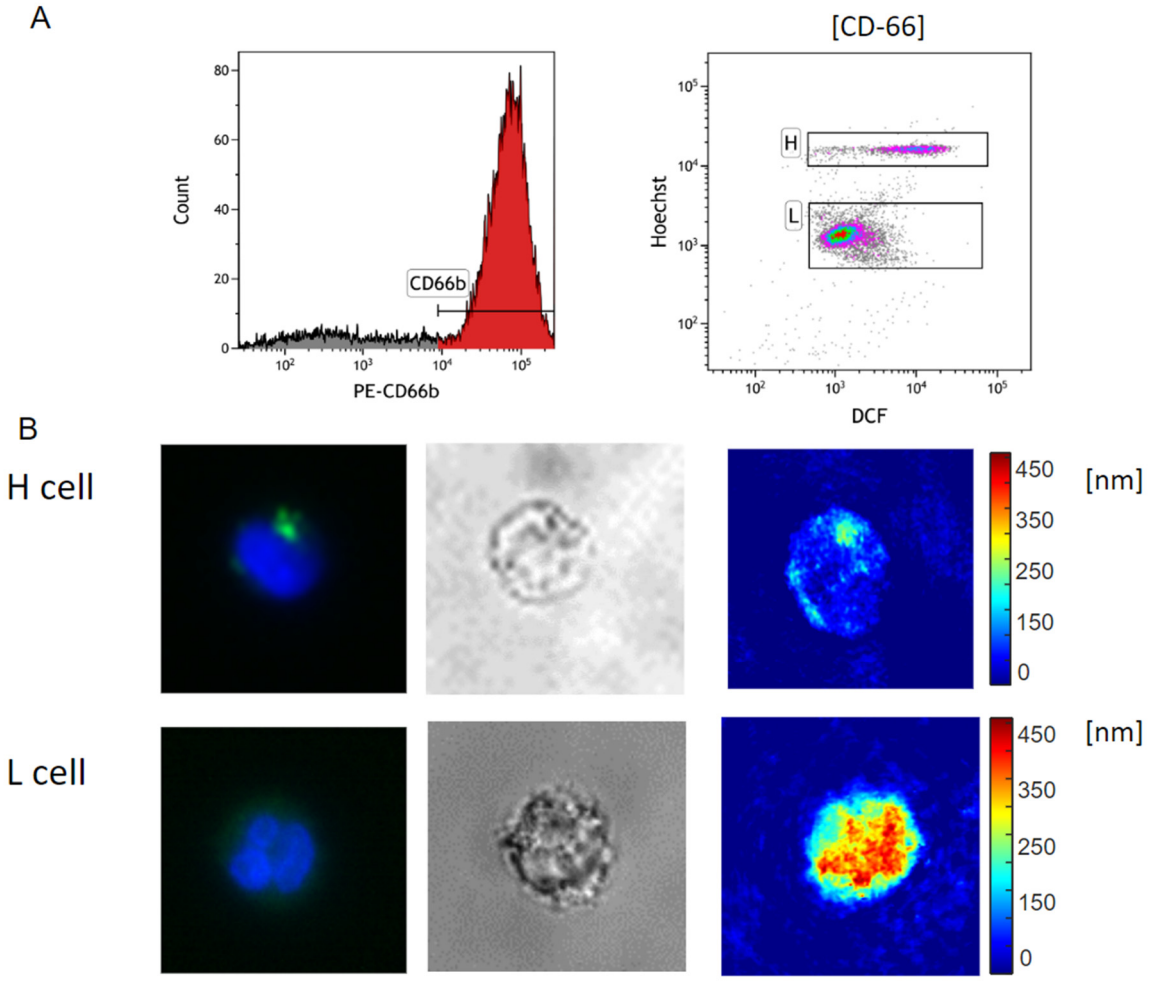

Figure 3. Sorting of high-Hoechst (H) and low-Hoechst (L) cells. (A) Neutrophils isolated from a healthy donor (BBD-11) were gated by CD66b expression. The gated cells are displayed on a DFC vs Hoechst dot plot. The two subpopulations of cells, H and L cells, were sorted for future analysis by the level of fluorescence and were isolated and fixated. (B) A representative cell from each subpopulation, as imaged by fluorescent microscopy with Hoechst (blue) and DFC (green) stains, brightfield, and IPM. Results indicate H cells are characterized by a round nucleus, focal DFC spots and low OPD in the nucleus. In comparison, L cells are characterized by a polymorphic nucleus, low-level and dispersed DFC, and high OPD in the nucleus.

Overall at this stage, 94 L cells and 77 H cells were captured. The cell images were converted to the label-free OPD maps and analyzed to extract different morphological parameters; two 2D parameters: cell area and cell perimeter, and two 3D parameters: average OPD and dry mass. Results from the 2D label-free parameters show no statistically significant differences between the two cell types: for cell area results are 100 vs. 98 μm2 for H and L cells, respectively, and for cell perimeter 54

 doi:10.20944/preprints202401.1554.v1

vs. 51 μm for H and L cell, respectively. In contrast, 3D label-free parameters show statistically significant differences between the two cell types: average OPD of 120 vs 200 nm OPD and dry mass 59 vs. 96 μg for H and L cells, respectively, with $p<0.0001$ in both cases (Figure 4A).

In order to determine the threshold of dry mass that best distinguishes between the H and L cell populations, we computed the cumulative distribution function (CDF) of cell dry mass for both cell populations. The CDF of L cells and H cells were plotted (as shown in Figure 4B) and the dry mass at which the two curves intersect was selected as the threshold that optimally separates these cell populations. This procedure was repeated for the average OPD, thereby yielding dry mass and average OPD thresholds of 73 μg and 161 μm, respectively, for distinguishing between the H and L cells. The accuracies of dry mass and OPD-based classification using these thresholds were 88% and 90%, respectively.

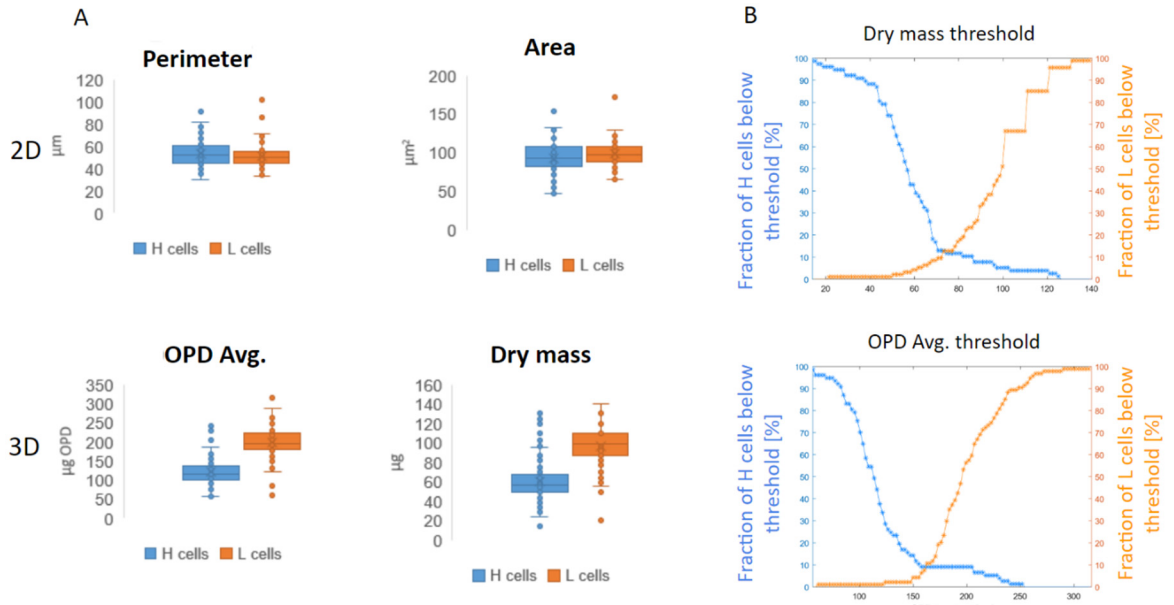

Figure 4. 2D and 3D parameter statistics. Neutrophils were isolated from healthy BBDs and sorted by FACS to H and L cells. The cells were captured by IPM and OPD maps of these cells were used to calculate 2D parameters (perimeter and area) and 3D parameters (average OPD and dry mass) in the two cell groups. Results show no statistically significant differences when comparing H and L cells in the 2D parameters; however, the 3D parameters are statistically significant ($p<0.0001$) (A). In order to determine the optimal threshold to differentiate the H and L cells a CDF chart was used. The optimal threshold is the intersection point of the two curves: 73 pg and 161 nm OPD for the dry mass and average OPD, respectively (B).

3.3. Capturing of neutrophils from healthy BBDs and MDS patients

Blood samples from 8 healthy BBDs and 5 MDS patients were analyzed. Neutrophils were isolated and the cells were stained by Hoechst and fixated by 1% PFA. Later, the cells were pumped into a microchannel at a rate of ~20 μl per hour. In case the cells were not visible as a result of sedimentation, the pumping speed is increased to 1000 μl / h for several minutes, afterwards the flow rate returned to 20 μl per hour. Theis low flow rate was necessary to ensure the cells flow on the bottom of the micro-channel, in the focal plane. The flowing cells were first visualized using the fluorescent microscopy for the imaging of the nucleus (using Hoechst), when a cell was identified it was also imaged by IPM.

The samples included 481 cells from MDS patients and 575 from BBDs. In order to exclude non-neutrophils from the analysis, cells that had a perimeter larger than the 95th percentile or smaller than the 5th percentile of sorted cells imaged were excluded. Thus, 438 neutrophils were analyzed for MDS patients and 384 for BBDs. Next, we used the threshold that was determined in Figure 3B in order to discriminate between H and L neutrophils using the dry mass. The differences in dry mass

 doi:10.20944/preprints202401.1554.v1

and average OPD dispersion pattern (Figure 5A and 5B, respectively) indicates on the present of the H cells subpopulation mostly in BBDs, these cells are characterized by dry mass or average OPD values below the threshold determined in Figure 4b.

Thus, among the BBDs, 21% of neutrophils are H cells, whereas in MDS patients only 4% are H cells (Figure 3C). The differences between the two groups were found to be statistically significant ($p < 0.001$)

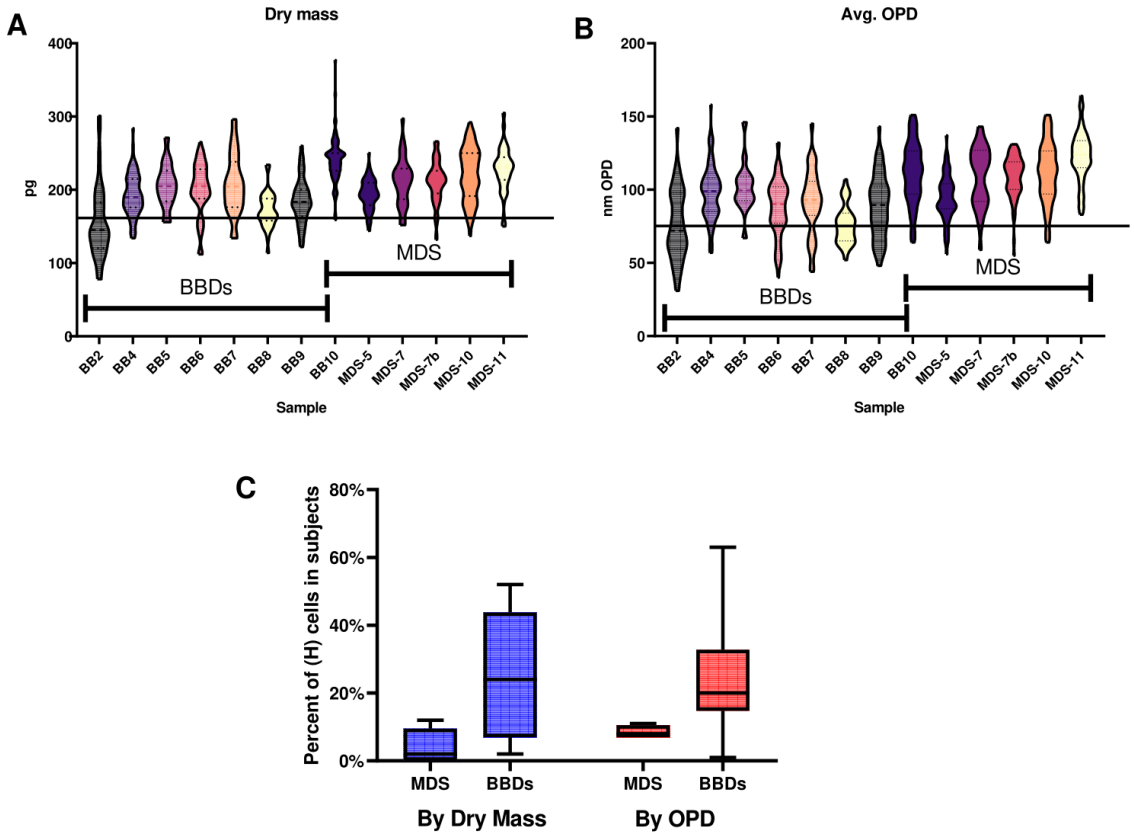

Figure 5. Violin plot charts of dry mass (A) and average OPD (B) of cells in the different MDS patients and BBDs. In both (A) and (B) the horizontal line represents the threshold between L and H cells. The percentage of H cells in MDS patients and BBDs is presented in (C) is significantly different.

4. Discussion

The diagnosis of MDS is a significant challenge in the current medical setting. In order to initiate the diagnostic process, the attending physician must first detect and interpret correctly the red flags that indicate the potential for MDS. The red flags include slowly progressing fatigue, bleeding infections and normocytic or macrocytic anemia. Only after these red flags are sighted will the patient be referred for a bone marrow aspiration and biopsy in order to diagnose MDS conclusively. However, these red flags are very ambiguous and several years may pass until they are interpreted correctly by the attending physician.

The most common method for routine diagnosis of hematological pathologies is complete blood count (CBC), which measures cell volume based on combination of electrical impedance and scatter analysis as well as non-specific fluorescence labels to provide automated, low-cost, fast, and fairly reliable estimated 5-part differential counting of WBCs: neutrophils, monocytes, eosinophils, basophils, and lymphocytes. However, for the more-detailed morphological analyses of WBCs needed to diagnose MDS, a blood smear is needed, as this test can detect morphological abnormalities such as nuclear hyper-segmentation and cytoplasmic hypo-granularity [7]. In a blood smear, usually manual analysis under a light microscope is carried out, which is a labor-intensive method requiring

 doi:10.20944/preprints202401.1554.v1

skilled technicians and can take a long time [22]. This delayed diagnosis can result in the loss of therapeutic opportunities. For example, for higher-risk MDS patients, hematopoietic cell transplantation is a potential curative treatment, but it is available only for patients in a good physical condition only [10]. In addition, delayed diagnosis might delay the onset of palliative treatment that may improve quality of life [23]. Current translational research of MDS focuses in understanding the role of various genetic and epigenetic factors as prognostic or predictive markers to influence treatment. However, to date, these factors have little influence on treatment [24]. Our work presents a low-cost and low-skill, automated and high-throughput approach for the raising of a red flag for MDS diagnosis. Employing our approach may improve quality of life and survival of these patients.

In MDS patients, neutrophils may be deficient not only in number but also in anti-microbial functionality [25]. These functional impairments in neutrophils increase the risk of severe infections, and infection-related deaths in MDS patients [5]. The functional deficiency of MDS neutrophils may be the result of hypogranularity, which is a feature of MDS and other myeloid malignancies [26]. Our work demonstrates the decrease in granules in MDS patients as evidenced by the reduced presence of DCF-stained granules in neutrophils from MDS patients compared to BBDs.

Using flow cytometry, IPM and fluorescence microscopy we examined morphological differences between neutrophils derived from MDS patients and those obtained from healthy donors. When examining neutrophils from MDS patients and BBDs in flow cytometry using stains for ROS (FDC) and DNA (Hoechst) a distinct pattern is observed. In BBDs, two cell clusters appear: one with higher Hoechst (H cells) and another with lower Hoechst (L cells In contrast, MDS patients presented only the cluster of cells with lower Hoechst). The most likely reason for the difference between the two groups is different states of DNA de-condensation, which effect the fluorescence by Hoechst staining [27,28]. Interestingly, the H cells, found almost exclusively in the BBDs, are usually diverse in the quantity of ROS presented in a single donor and the average ROS expression differs from sample to sample compared to the ROS in the L cells. This may suggest that the different BBDs presented different activation levels of the immune system during the time of donation. The fact that most MDS patients had no H cell cluster suggests a defective activation of the immune system. This correlates with the high rate of infections MDS patients endure [5,29]. One possible explanation for the H cell population, found mostly in BBDs, is that these cells represent stimulated neutrophils that produce extracellular structures called neutrophil extracellular traps (NETs) [30]. During infection, neutrophils may swallow microorganisms by phagocytosis, following which the microorganisms are exposed to antimicrobial peptides, enzymes and ROS. These components neutralize and kill the protruding microorganisms, effectively preventing widespread infections [31]. In addition to phagocytosis and intracellular killing of pathogens, neutrophils are capable of neutralizing microorganisms by NETs [32]. In this mechanism, the neutrophil secrets chromatin, including DNA and histones, to the extracellular area, thus trapping pathogenic microorganisms. This process is dependent on the generation of ROS by NADPH oxidase [33]. In a recently published work it was shown that neutrophils derived from MDS patients have markedly diminished NET-forming capacity than age-adjusted healthy controls; neutrophils from healthy controls present more chromatin decondensation and more ROS secretion of NETs in reaction to stimuli compared to neutrophils from MDS patients [34]. These results are in correlation with our morphological findings: the activation of the NET mechanism in BBDs but not in MDS patients is supported by the fact that H cells (found almost exclusively in BBDs) present higher Hoechst values suggesting chromatin decondensation, and the presence of DFC staining is suggestive of ROS production. Decondensed DNA may also be the reason for the low OPD values of the nucleus in H cells.

Our research has three main limitations. First, blood bank donors are not the ideal healthy control to MDS patients based on the differences in age. Second, a larger cohort of patients should be used in future research to strengthen our findings. Third, the study includes only high-risk MDS cases, Initial results in low-risk MDS cases suggest that neutrophils in this condition present H cells. A more comprehensive comparison between high and low MDS cells or anemia of unknow origin using IPM can be performed in future research.

5. Conclusions

To date, automated CBC is the most commonly used tool for the diagnosis of hematological pathologies. For more detailed morphological description of WBCs, manual analysis is needed, which is a labor-intensive method requiring skilled technicians and takes a long time to produce results. An IPM system integrated with a microfluidic mechanism has been shown to provide additional information on subtypes of WBCs that cannot be obtained by other automated methods, and can potentially raise a red flag for MDS sooner. To our knowledge, this is the first work in which IPM has been used to distinguish between two WBCs of the same lineage in different developmental stages and thereby diagnose a medical condition; thus this technique may be applicable to numerous other pathologies.

Author Contributions: Conceptualization, I.B. and L.L.; methodology, I.B. and O.D.; software, A.G.; validation, I.B., L.L. and N.T.S.; formal analysis, I.B.; investigation, I.B., L.L.; resources, N.T.S.; data curation, I.B.; writing—original draft preparation, I.B.; writing—review and editing, N.T.S.; visualization, I.B.; supervision, N.T.S.; project administration, O.D.; funding acquisition, N.T.S. All authors have read and agreed to the published version of the manuscript.

Funding: This research received no external funding.

Institutional Review Board Statement: The study was conducted in accordance with the Declaration of Helsinki, and approved by the Institutional Review Board of the Sheba Medical Center (protocol code 8374-21-SMC, date of approval: 14.7.2021) and the Ethics Committee of the Tel Aviv University (protocol code 3618-2 date of approval: 3.10.2021) for studies involving humans.

Informed Consent Statement: Informed consent was obtained from all subjects involved in the study.

Data Availability Statement: Dataset available on request from the authors.

Conflicts of Interest: The authors declare no conflicts of interest.

References

1. Sekeres MA, Taylor J. Diagnosis and Treatment of Myelodysplastic Syndromes: A Review. JAMA. 2022 Sep 6;328(9):872-880. doi: 10.1001/jama.2022.14578. PMID: 36066514.
2. Arber DA, Orazi A, Hasserjian R, Thiele J, Borowitz MJ, Le Beau MM, Bloomfield CD, Cazzola M, Vardiman JW. The 2016 revision to the World Health Organization classification of myeloid neoplasms and acute leukemia. Blood. 2016 May 19;127(20):2391-405. doi: 10.1182/blood-2016-03-643544. Epub 2016 Apr 11. PMID: 27069254.
3. Pang WW, Pluvinage JV, Price EA, Sridhar K, Arber DA, Greenberg PL, Schrier SL, Park CY, Weissman IL. Hematopoietic stem cell and progenitor cell mechanisms in myelodysplastic syndromes. Proc Natl Acad Sci U S A. 2013 Feb 19;110(8):3011-6. doi: 10.1073/pnas.1222861110. Epub 2013 Feb 6. PMID: 23388639; PMCID: PMC3581956.
4. Neukirchen J, Blum S, Kuendgen A, Strupp C, Aivado M, Haas R, Aul C, Gattermann N, Germing U. Platelet counts and haemorrhagic diathesis in patients with myelodysplastic syndromes. Eur J Haematol. 2009 Nov;83(5):477-82. doi: 10.1111/j.1600-0609.2009.01299.x. Epub 2009 Jun 22. PMID: 19548919.
5. Nachtkamp K, Stark R, Strupp C, Kündgen A, Giagounidis A, Aul C, Hildebrandt B, Haas R, Gattermann N, Germing U. Causes of death in 2877 patients with myelodysplastic syndromes. Ann Hematol. 2016 May;95(6):937-44. doi: 10.1007/s00277-016-2649-3. Epub 2016 Mar 30. PMID: 27025507.
6. Moretti S, Lanza F, Spisani S, Latorraca A, Rigolin GM, Giuliani AL, Castoldi GL, Traniello S. Neutrophils from patients with myelodysplastic syndromes: relationship between impairment of granular contents, complement receptors, functional activities and disease status. Leuk Lymphoma. 1994 May;13(5-6):471-7. doi: 10.3109/10428199409049637. PMID: 8069192.
7. Shekhar R, Srinivasan VK, Pai S. How I investigate dysgranulopoiesis. Int J Lab Hematol. 2021 Aug;43(4):538-546. doi: 10.1111/ijlh.13607. Epub 2021 May 25. PMID: 34031992.
8. Fuhler GM, Hooijenga F, Drayer AL, Vellenga E. Reduced expression of flavocytochrome b558, a component of the NADPH oxidase complex, in neutrophils from patients with myelodysplasia. Exp Hematol. 2003 Sep;31(9):752-9. doi: 10.1016/s0301-472x(03)00188-7. PMID: 12962720.

9. Arber DA, Orazi A, Hasserjian R, Thiele J, Borowitz MJ, Le Beau MM, Bloomfield CD, Cazzola M, Vardiman JW. The 2016 revision to the World Health Organization classification of myeloid neoplasms and acute leukemia. Blood. 2016 May 19;127(20):2391-405. doi: 10.1182/blood-2016-03-643544. Epub 2016 Apr 11. PMID: 27069254.
10. Cutler CS, Lee SJ, Greenberg P, Deeg HJ, Pérez WS, Anasetti C, Bolwell BJ, Cairo MS, Gale RP, Klein JP, Lazarus HM, Liesveld JL, McCarthy PL, Milone GA, Rizzo JD, Schultz KR, Trigg ME, Keating A, Weisdorf DJ, Antin JH, Horowitz MM. A decision analysis of allogeneic bone marrow transplantation for the myelodysplastic syndromes: delayed transplantation for low-risk myelodysplasia is associated with improved outcome. Blood. 2004 Jul 15;104(2):579-85. doi: 10.1182/blood-2004-01-0338. Epub 2004 Mar 23. PMID: 15039286.
11. Miceli MV, Liles MR, Newsome DA. Evaluation of oxidative processes in human pigment epithelial cells associated with retinal outer segment phagocytosis. Exp Cell Res. 1994 Sep;214(1):242-9. doi: 10.1006/excr.1994.1254. PMID: 8082727.
12. Uberti AF, Olivera-Severo D, Wassermann GE, Scopel-Guerra A, Moraes JA, Barcellos-de-Souza P, Barja-Fidalgo C, Carlini CR. Pro-inflammatory properties and neutrophil activation by Helicobacter pylori urease. Toxicon. 2013 Jul;69:240-9. doi: 10.1016/j.toxicon.2013.02.009. Epub 2013 Mar 1. PMID: 23466444.
13. Bland EJ, Keshavarz T, Bucke C. Using 2', 7'-dichlorodihydrofluorescein-diacetate to assess polysaccharides as immunomodulating agents. Mol Biotechnol. 2001 Oct;19(2):125-31. doi: 10.1385/MB:19:2:125. PMID: 11725482.
14. Merchant R, Gandhi G, Allahbadia GN. In vitro fertilization/intracytoplasmic sperm injection for male infertility. Indian J Urol. 2011 Jan;27(1):121-32. doi: 10.4103/0970-1591.78430. PMID: 21716935; PMCID: PMC3114573.
15. Girshovitz P, Shaked NT. Generalized cell morphological parameters based on interferometric phase microscopy and their application to cell life cycle characterization. Biomed Opt Express. 2012 Aug 1;3(8):1757-73. doi: 10.1364/BOE.3.001757. Epub 2012 Jun 29. PMID: 22876342; PMCID: PMC3409697.
16. Mirsky SK, Barnea I, Levi M, Greenspan H, Shaked NT. Automated analysis of individual sperm cells using stain-free interferometric phase microscopy and machine learning. Cytometry A. 2017 Sep;91(9):893-900. doi: 10.1002/cyto.a.23189. Epub 2017 Aug 22. PMID: 28834185.
17. Nissim N, Dudaie M, Barnea I, Shaked NT. Real-Time Stain-Free Classification of Cancer Cells and Blood Cells Using Interferometric Phase Microscopy and Machine Learning. Cytometry A. 2021 May;99(5):511-523. doi: 10.1002/cyto.a.24227. Epub 2020 Oct 13. PMID: 32910546.
18. Ugele M, Weniger M, Stanzel M, Bassler M, Krause SW, Friedrich O, Hayden O, Richter L. Label-Free High-Throughput Leukemia Detection by Holographic Microscopy. Adv Sci (Weinh). 2018 Oct 11;5(12):1800761. doi: 10.1002/advs.201800761. PMID: 30581697; PMCID: PMC6299719.
19. Noy L, Barnea I, Mirsky SK, Kamber D, Levi M, Shaked NT. Sperm-cell DNA fragmentation prediction using label-free quantitative phase imaging and deep learning. Cytometry A. 2023 Jun;103(6):470-478. doi: 10.1002/cyto.a.24703. Epub 2022 Nov 23. PMID: 36333835.
20. Rongli G, Barnea I, Shaked NT. Low-coherence shearing interferometry with constant off-axis angle. Frontiers in Physics 8 (2021): 611679.
21. Girshovitz P, Shaked NT. Fast phase processing in off-axis holography using multiplexing with complex encoding and live-cell fluctuation map calculation in real-time. Opt Express. 2015 Apr 6;23(7):8773-87. doi: 10.1364/OE.23.008773. PMID: 25968715.
22. Chabot-Richards DS, George TI. White blood cell counts: reference methodology. Clin Lab Med. 2015 Mar;35(1):11-24. doi: 10.1016/j.cll.2014.10.007. Epub 2014 Dec 4. PMID: 25676369.
23. Madanat Y, Sekeres MA. Optimizing the use of hypomethylating agents in myelodysplastic syndromes: Selecting the candidate, predicting the response, and enhancing the activity. Semin Hematol. 2017 Jul;54(3):147-153. doi: 10.1053/j.seminhematol.2017.06.001. Epub 2017 Jun 23. PMID: 28958288.
24. Platzbecker U. Treatment of MDS. Blood. 2019 Mar 7;133(10):1096-1107. doi: 10.1182/blood-2018-10-844696. Epub 2019 Jan 22. PMID: 30670446.
25. Martin S, Baldock SC, Ghoneim AT, Child JA. Defective neutrophil function and microbicidal mechanisms in the myelodysplastic disorders. J Clin Pathol. 1983 Oct;36(10):1120-8. doi: 10.1136/jcp.36.10.1120. PMID: 6311878; PMCID: PMC498487.

26. Watson N, Dunlop L, Robson L, Sharma P, Smith A. 17p- syndrome arising from a novel dicentric translocation in a patient with acute myeloid leukemia. Cancer Genet Cytogenet. 2000 Apr 15;118(2):159-62. doi: 10.1016/s0165-4608(99)00188-0. PMID: 10748299.
27. Pithon-Curi TC, Schumacher RI, Freitas JJ, Lagranha C, Newsholme P, Palanch AC, Doi SQ, Curi R. Glutamine delays spontaneous apoptosis in neutrophils. Am J Physiol Cell Physiol. 2003 Jun;284(6):C1355-61. doi: 10.1152/ajpcell.00224.2002. Epub 2003 Jan 15. PMID: 12529242.
28. Wang Y, Li M, Stadler S, Correll S, Li P, Wang D, Hayama R, Leonelli L, Han H, Grigoryev SA, Allis CD, Coonrod SA. Histone hypercitrullination mediates chromatin decondensation and neutrophil extracellular trap formation. J Cell Biol. 2009 Jan 26;184(2):205-13. doi: 10.1083/jcb.200806072. Epub 2009 Jan 19. PMID: 19153223; PMCID: PMC2654299.
29. Toma A, Fenaux P, Dreyfus F, Cordonnier C. Infections in myelodysplastic syndromes. Haematologica. 2012 Oct;97(10):1459-70. doi: 10.3324/haematol.2012.063420. Epub 2012 Jun 24. PMID: 22733024; PMCID: PMC3487546.
30. Brinkmann V, Zychlinsky A. Beneficial suicide: why neutrophils die to make NETs. Nat Rev Microbiol. 2007 Aug;5(8):577-82. doi: 10.1038/nrmicro1710. PMID: 17632569.
31. Hampton MB, Kettle AJ, Winterbourn CC. Inside the neutrophil phagosome: oxidants, myeloperoxidase, and bacterial killing. Blood. 1998 Nov 1;92(9):3007-17. PMID: 9787133.
32. Brinkmann V, Reichard U, Goosmann C, Fauler B, Uhlemann Y, Weiss DS, Weinrauch Y, Zychlinsky A. Neutrophil extracellular traps kill bacteria. Science. 2004 Mar 5;303(5663):1532-5. doi: 10.1126/science.1092385. PMID: 15001782.
33. Fuchs TA, Abed U, Goosmann C, Hurwitz R, Schulze I, Wahn V, Weinrauch Y, Brinkmann V, Zychlinsky A. Novel cell death program leads to neutrophil extracellular traps. J Cell Biol. 2007 Jan 15;176(2):231-41. doi: 10.1083/jcb.200606027. Epub 2007 Jan 8. PMID: 17210947; PMCID: PMC2063942.
34. Brings C, Fröbel J, Cadeddu P, Germing U, Haas R, Gattermann N. Impaired formation of neutrophil extracellular traps in patients with MDS. Blood Adv. 2022 Jan 11;6(1):129-137. doi: 10.1182/bloodadvances.2021005721. PMID: 34653237; PMCID: PMC8753191.